High-quality GeV proton beam generation by triple-lasers plasma interaction

Obaydur Rahman[1,2,a] and Zheng-Mao Sheng[1,b]
[1] *Department of Physics, Institute for Fusion Theory and Simulation, Zhejiang University, Hangzhou 310027, China*
[2] *Department of Physics, Mawlana Bhashani Science and Technology University, Tangail 1902, Bangladesh*

A novel scheme of proton acceleration is investigated to enhance the proton beam quality using triple-laser pulses double-layer target interaction via particle-in-cell simulations. In this scheme, three linearly polarized Gaussian laser pulses are used to irradiate the target from different angles. The prime role of the identical oblique laser pulses not only forms hot-electron bunches but also reduces the reflection of the succeeding pulse by changing the pre-target electron distributions. The main pulse is then self-focused resulting in an enhanced energy coupling from the laser to the plasma electrons. These high-energetic hot electrons induce a much stronger electrostatic field towards the longitudinal direction. As a result, a high-quality proton beam of ∼1.2 GeV peak energy with immensely low energy spread ∼ 4% and small divergence ∼ 5° can be obtained at intensities of 10^{21} Wcm^{-2}, which is one order lower compared with recently proposed some other schemes.

I. INTRODUCTION

The study of laser-plasma interaction to optimize the ion acceleration has received considerable attention over the last few decades due to its extensive potential applications, including medical physics, fast ignition in inertial confinement fusion, nuclear physics, proton radiography, isotope production, and for probing radiation-induced processes in matter[1–5]. However, most of the applications demand high energy ion beam as well as high energy coupling from laser to ion than currently attainable, and many require narrow beam spread and beam divergence. For example, to treat cancer cells using hadron therapy requires proton beams of about 200MeV with energy spread $\leq 2\%$ in order to protect neighboring healthy tissues[6]. Usually, laser-driven ion beams are in most cases broad besides few ions can reach the maximum energy, which limits their use in practical applications. Therefore, to enhance the ion beam quality in order to make it feasible for such applications numerous theoretical and experimental investigations have been proposed, yet, to date, the attained ion beam energies are not sufficient for some applications. Several mechanisms, depending on the design of the laser-plasma interaction, have been reported to realize the laser-driven ion acceleration, such as target normal sheath acceleration (TNSA)[7–9], radiation pressure acceleration (RPA)[10–12], breakout after-burner (BOA)[13,14], shock acceleration[15], Coulomb explosion[1], etc.

Recently, divers attempts have been conducted to generate GeV proton beams using intense laser-plasma interactions as presented in Table I. It is seen that a highly intense laser pulse of intensity $\geq 10^{22}\mathrm{Wcm}^{-2}$ is required both for linearly and circularly polarized laser pulses. Although the GeV ion beam can be produced using conventional accelerators such as rf accelerators however the production cost is extremely high as well as needs large space, for example, the cost and size of the Large Hadron Collider (LHC) are about 7.5 billion euro and 27 km, respectively. Therefore, the interest in the laser-driven accelerator is driven by means of their compactness and lower cost. Moreover, it can produce ion beams with a higher charge, a smaller divergence, and with a very short duration of the order of a few ps. The use of double-layer targets in this field has charmed a lot of attention since they can promote the laser absorption as well as to reduce the target deformation due to the shock wave hence to improve the beam quality[11,12,16–18]. In addition, the multi-laser pulses scheme has been reported in some recent studies[18–24] to gain additional control over the ion beam properties. It has shown by experiments that the maximum proton energy and the laser to proton energy conversion efficiency can be significantly enhanced using the multi-laser pulses scheme[21–23].

	Laser Intensity (Wcm^{-2})	Energy (GeV)
Y. J. Gu *et al.*	2.13×10^{22}	1.00 (LP)
Y. J. Gu *et al.*	2.13×10^{22}	1.67 (LP)
X. Zhang *et al.*	1.37×10^{22}	1.22 (CP)
W. Zhou *et al.*	3.95×10^{22}	1.30 (CP)
D. B. Zou *et al.*	2.74×10^{22}	1.50 (CP)
Z. M. Zhang *et al.*	2.76×10^{22}	1.00 (CP)
Z. M. Zhang *et al.*	3.90×10^{22}	4.20 (CP)
Y. Xu *et al.*	5.50×10^{22}	1.31 (CP)
B. Qiao *et al.*	6.30×10^{22}	1.35 (CP)
M. Chen *et al.*	2.76×10^{22}	1.20 (CP)
Present scheme	$\mathbf{2.26 \times 10^{21}}$	**1.20 (LP)**

TABLE I. Several attempts to generate GeV proton bunch from laser-plasma interactions with different laser and target parameters[10–12,25–31].

In this paper, we have proposed a novel triple-laser pulses (TLP) double-layer target interaction scheme to enhance the proton beam energy up to GeV with significantly low energy spread using one order lower in-

[a] armanphy203@gmail.com
[b] zmsheng@zju.edu.cn

tense laser pulse as compared with the recently proposed some other schemes those mentioned in table I. The present scheme is quite different from those reported in Refs.[18–24]. They have considered either normal or oblique irradiation of the target while the mixed irradiation is considered here to gain additional control over the proton beam qualities.

II. LASER AND TARGET PARAMETERS

Two-dimensional particle-in-cell (PIC) simulation code Opic2.0[11,18,19] is used to investigate the proposed scheme. A double-layer target is considered which consists of a highly dense ($n_e = 24n_c$) thick carbon layer (CL) pre-target and a critically dense ($n_e = 1n_c$) thin hydrogen layer (HL) rear-target, where $n_c = m_e\omega^2/4\pi e^2$ is the critical density with e, m_e, and ω being the electron charge, electron mass, and laser frequency, respectively. The rest mass of carbon ions is set to $m_c = 12m_p$, where $m_p = 1836m_e$ is the proton mass. The role of the CL is to protect the target from the unusual deformation caused by the shock wave generated due to intense laser pulse and supplies sufficient electrons for acceleration. Three linearly p-polarized Gaussian laser pulses (a_1, a_2 and a_3) of each having wavelength $\lambda = 1\mu$m, waist $W_0 = 5\lambda$, and pulse duration $\tau = 40T$ with $T = 3.3$ fs being the laser period, are used to irradiate the target from the left side of the simulation box. The electric field of the laser light (for each pulse) is[19]

$$E_y(x,y,t) = a_0\sqrt{W_0/W(x)}e^{-\frac{(y-y_0)^2}{W^2(x)}}e^{-\frac{(t-2\tau_0)^2}{2\tau_0^2}}e^{i(kx-\omega t)}$$

where $W(x) = W_0\sqrt{1+(x/x_0)^2}$ and $\tau_0 = \tau/1.665$. The corresponding normalized laser amplitudes are $a_1 = a_2 = 5$ ($I_1 = I_2 = 3.4\times10^{19}$ Wcm^{-2}) and $a_3 = 40$ ($I_3 = 2.2\times10^{21}$ Wcm^{-2}). At first, two identical lower intense laser pulses (a_1 and a_2) strike the pre-target obliquely at the same time. The optimal angle between a_1 and a_2 is 2θ with $\theta = \pm30°$, with respect to the x-axis, and is consistent with that reported in Ref.[18]. After 80T, a highly intense main laser pulse (a_3) is launched normally to the previously irradiated target. The distance of a_1 and a_2 from the center of a_3 at the starting point is $d_0/2$ with $d_0 = 29.4\lambda$. The other optimum parameters are $D = 10\lambda$, $d_1 = 5\lambda$, $d_2 = 0.05\lambda$, and $d_3 = 60\lambda$, where the symbols represent their usual meanings. In order to observe the long-distance propagation of the main pulse, a moving window with 6000 (x) × 750 (y) cells is used to reduce the computational loads. The number of macro-particles per cell for the CL and HL are 20 and 10, respectively.

To demonstrate the effectiveness as well as to increase the reliability of the proposed TLP scheme, two other cases are also considered using the identical laser and target parameters, in the simulations as follows:

- **Double-laser pulses (DLP):** Two consecutive p-polarized laser pulses are used to irradiate the target normally. The time interval between these two pulses is 40T. The normalized amplitudes are $a_1' = a_1 + a_2$ and $a_2' = a_3$ for the first and second pulses, respectively.

- **Single-laser pulse (SLP):** A single p-polarized laser pulse is used to irradiate the target normally. The normalized amplitude is $a = \sum_{n=1}^{N} a_n$, where N is number of pulses used in the TLP scheme.

The corresponding laser energy $E_L = \sum_{n=1}^{N} I_0\pi r_n^2 a_n^2 \tau_n$, where $r = W_0/2\sqrt{ln2}$ and $I_0 = 1.37\times10^{18}$Wcm^{-2}, are 127.8J, 87J, and 84.4J for the SLP, DLP, and TLP cases, respectively. The sketches of theses three cases are depicted in Fig. 1.

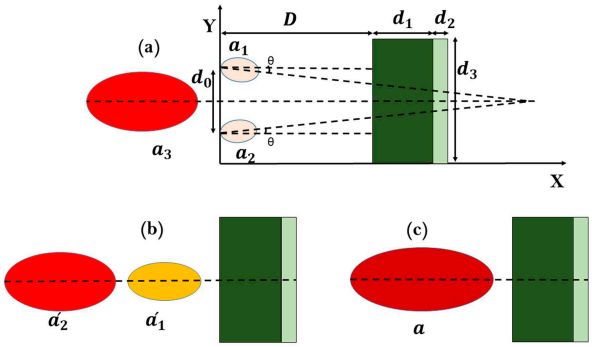

FIG. 1. (a) Schematic of the triple-laser pulses (TLP) scheme. Three laser pulses are launched from the left side of the simulation box. The corresponding amplitudes are defind as a_1, a_2, and a_3, where $a_1 = a_2 < a_3$. The incidence angles for these three pulses are $+30°$, $-30°$, and $0°$, respectively, with respective to the x axis. The symbols d_0, D, d_1, d_2, and d_3 represent the usual meanings as depicted on the Fig. 1(a). The schematics of (b) double-laser pulses (DLP) and (c) single-laser pulse (SLP) cases.

III. ROBUSTNESS OF PROTON BEAM DUE TO TLP

The benefits of employing the lower intense oblique laser pulses in laser-driven proton acceleration are shown in Fig. 2. In this paper, the green, red, and blue lines represent the SLP, DLP, and TLP cases, respectively, otherwise will be mentioned in the text. Figure 2(a) shows the time-integrated energy spectra of protons of the above mentioned three cases at 350T. One can see that the proposed TLP scheme significantly enhances the proton beam energy as well as the number of high-energetic protons. The PIC simulations results have demonstrated that a monoenergetic proton beam of ∼1.2 GeV peak energy can be achieved using one order of lower intense laser pulse than that reported in Table I. Furthermore,

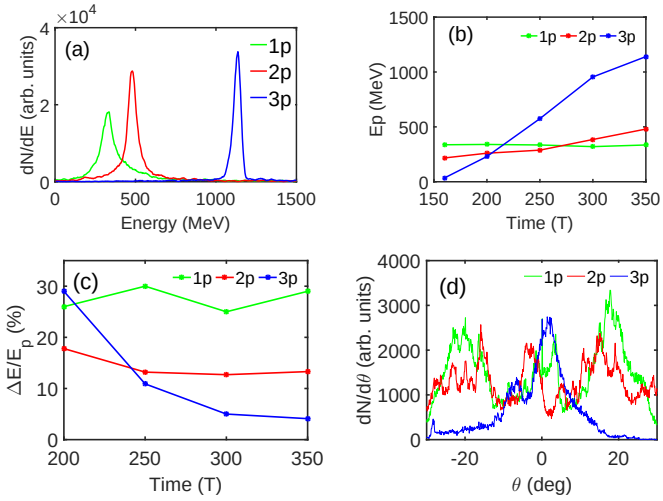

FIG. 2. (a) The energy spectra, (b) temporal evolution of the peak energy, (c) temporal evolution of the energy spread, and (d) the angular energy spectra of the accelerated protons obtained from the above mentioned (see Fig. 1) three cases. Note that a much better quality high energy proton beam can be achieved for the TLP case as compared with the other two cases.

it is also shown that the peak energy is about 3.6 and 2.5 times higher, i.e., an increase of more than 250% and 150% as compared with the SLP and DLP cases, respectively. Figure 2(b) shows that the enhancement of the proton beam peak energy with time is very rapid for the TLP case. This indicates the stable and longer time propagation of the proton beam. This is expected since the main pulse becomes much more effective at later time due to the longer time delay. In contrast, the peak energy remains unchanged for the SLP case while slightly increases for the DLP case. It is important to note that the energy spread characterized by $\Delta E/E_p$, where E_p and ΔE are the peak and full width at half maximum (FWHM) proton energies, respectively, decreases speedily with time for the TLP case while slightly decreases for the other cases as shown in Fig. 2(c). In fact, the obtained lowest energy spreads are 29% (SLP), 13.3% (DLP), and 4% (TLP), revealing an improved quality proton beam for the TLP case. Figure 2(d) shows the angular spectra of the proton beam. This figure indicates that the beam divergence is also significantly reduced and a single-peaked, near the zero angle, angular spectrum of $\sim 5^\circ$ angular spread at FWHM is found for the TLP case while for the other two cases multiple peaks with relatively larger angular spreads are observed. The lower divergence angle, corresponding to the TLP case, means that the beam transverse divergence is greatly suppressed and the generated proton beam is mainly accelerated in the longitudinal direction, which predicts the good beam collimation. Whereas for other cases, the accelerated protons are diverged in the transverse direction due to the widely distributed hot-electron clouds. From this above results, it is seen that the TLP can produce a much better quality proton beam by means of lower laser energy as compared with the other two cases. These results have suggested that the TLP scheme could be an alternative choice than the high-energy laser pulses that are not readily available by the current state-of-the-art laser technology, and one can control beam quality efficiently. Up to this, the obtained findings are presented. In the following section, the main reasons behind these findings will be discussed.

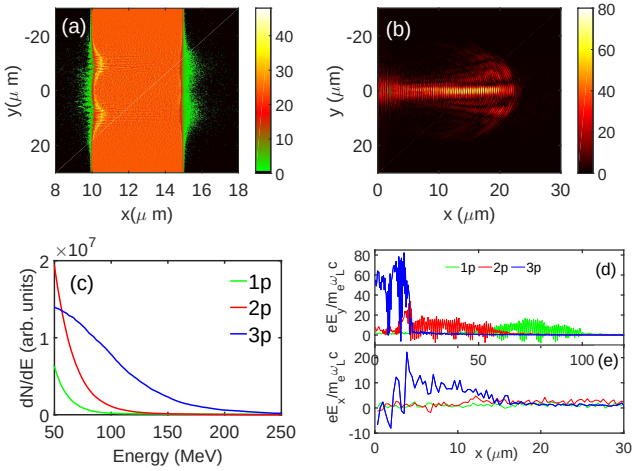

FIG. 3. (a) The pre-target electron distribution at 80T. It is seen that pre-target is fully ionized by the oblique laser-pulses before the arrival of the main pulse hence forming a microstructured target that contains two electron bunches. (b) The laser envelope E_y along the laser propagation axis at 160T for the TLP case. Note that the main laser pulse is self-focused towards the central axis. (c) The energy spectra of hot electrons at 160T. Only the forward-directed hot electrons (50 MeV -250 MeV) are considered. The transverse (d) and longitudinal (e) electric field plots at 160T.

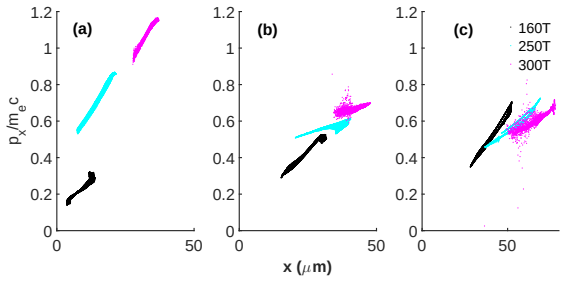

FIG. 4. Distribution of protons in phase space $(x-p_x)$ at different moments for (a) TLP case, (b) DLP case, and (d) SLP case, where p_x is the longitudinal proton momentum normalized by $m_e c$. The black, cyan, and magenta lines correspond to the moment at 160T, 250T, and 300T, respectively.

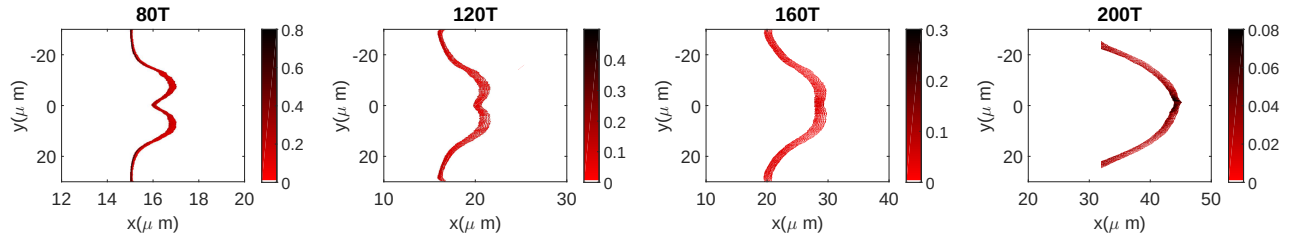

FIG. 5. Temporal evolution of the proton density distributions for the TLP case. Times are indicated on each figure. Note that the double peaked proton layer is merged into a highly dense single peaked at 200T.

IV. REASONS FOR PROTON BEAM ROBUSTNESS

We now consider the dynamics of the pre-target electrons which are very crucial for laser-driven ion acceleration. First of all, the pre-target is ionized by the oblique laser pulses hence turns into a microstructured target with near wavelength before the arrival of the main pulse as shown in Fig. 3(a), which represents the pre-target electron distributions at 80T. Several recent studies have been reported that the structured target drastically enhances the absorption of the incident laser beam consequently leads to an increase in the maximum proton beam energy[32,33]. Meanwhile, two hot-electron bunches are also produced by the oblique pulses due to vacuum heating[34] which propagates diagonally to the main laser axis. As time goes on, they merge into a highly dense single bunch[24] therefore form a weak sheath field at the rear side of the target. At this stage, the proton acceleration is tiny and is driven due to TNSA. It is also important to note that the target deformation at this time is very weak. The weakly deformed microstructured pre-target as well as the cone guiding effect provided by the diagonally propagating hot electrons bunches not only reduce the reflection[35] but also enhance the focusing of the succeeding laser pulse as shown in Fig. 3(b), which depicts the laser envelope E_y along the laser propagation axis at 160T. One can see that the intensity of the self-focused laser pulse is about four times higher than the main laser pulse, i.e. $I_f = 4I_3$ as shown in Fig. 3(d). The energy loss during the laser-plasma interaction is compensated by the energy concentration due to the laser self-focusing. The highly intense focused laser light can trap the pre-accelerated hot-electron bunch and accelerates them in the forward direction through direct laser acceleration by the intense radiation pressure similar to the so-called snowplow consequently boosts the energy coupling from the laser to the target electrons. It is worth noting that much of the laser pulses also remain near the target surface which suggests the longer time laser-plasma interaction. As a result, a significant amount of higher energetic hot electron is generated which prolongs the accelerating field. Figure 3(c) shows the time-integrated energy spectra of the hot electrons (50-250 MeV) generated at the rear-side of the target at 160T. It is shown that the energy spectra demonstrate an exponential dependence of $dN/dE \propto \exp(-E/T_h)$, where E and T_h represent the hot electron energy and temperature, respectively, for all cases. Using Maxwellian fitting, the hot-electron temperature is found to 41.5 MeV for the TLP case, which is about 2.5 (3.4) times higher than the DLP (SLP) case. The hot electron temperature is also higher than the widely used ponderomotive scaling, $T_p = [(1 + a^2/2)^{1/2} - 1]m_e c^2 = 13.65$ MeV. In addition, the number of higher energetic hot electrons is also larger as compared with other cases. Therefore, these larger number of high-temperature hot electrons will result in the enhancement of the accelerating sheath field according to $E_s \propto \sqrt{n_h T_h}$, where n_h is the number of hot electrons and T_h is the temperature of the hot electrons, in the target rear surface and is consistent with the results shown in Fig. 3(e), which presents the self-generated longitudinal electric field E_x at 160T. At this time, the amplitude of E_x is much higher for the TLP case than the other two cases. This strong sheath field induces an enhanced TNSA, which not only suppresses the proton beam divergence but also increases the maximum proton beam energy. Figure 4 shows the distribution of protons in phase space $x - p_x$ at different times for (a) TLP, (b) DLP, and (c) SLP cases. One can see that the longitudinal momentum of the proton is about 1.5 times higher than the other cases, which supports the enhancement of the sheath field as well as predicts the longer time laser-plasma interaction as discussed above.

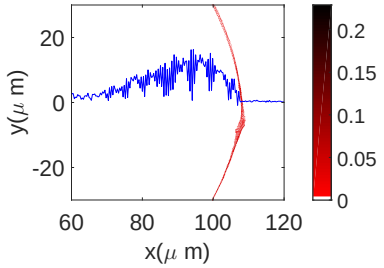

FIG. 6. The transverse electric field $eE_y/m_e\omega_L c$ (blue line) along with proton density distributions (red line) at 300T for the TLP case. Note that the proton layer co-moves with the laser pulse suggesting the existence of the laser breakout afterburner regime of proton acceleration. For a better view, we multiplied the E_y by 1/2.

Now we will illustrate the proton acceleration in detail. Figure 5 shows the temporal evolution of the proton distribution for the TLP case. In the early stage, the protons are mainly accelerated due to TNSA and the accelerating proton layer contains two density humps that are generated due to the above-mentioned electron bunches created by the oblique pulses. These high energetic density humps converge to form a single highly dense proton bunch as time goes on, as shown in the snapshot at 200T. Afterward, the merged highly dense proton layer rapidly co-propagates with the laser pulse in the forward direction, as shown in Fig. 6. As a result, the protons can be accelerated to very high energy with a relatively larger number of accelerated protons due to BOA. Intensive explanations about the BOA stage acceleration can be found in Refs.[13,14].

However, the proton acceleration process is quite different for other cases. The unusual target deformation is much higher for both cases due to the strong shock generated by the intense radiation pressure. As a result, such a structured target and the cone guiding effects were not noticed. Moreover, the self-focusing of the laser light could not found instead, the laser pulse completely scattered by the target. Although a strong sheath field was formed in the early stage, however, due to the transverse instability it rapidly decreased which reduced acceleration efficiency for these cases.

V. INFLUENCES OF PULSES INTENSITIES

The present investigation shows the effectiveness of employing the TLP scheme over that of the other schemes. Therefore, it is important to see how different laser pulses influence the proton acceleration. To do that, we have performed a series of simulations both for the oblique and normal pulses separately. The simulation parameters are the same as used before except:

- **Oblique Pulses:** a_1 and a_2 ($a_1 = a_2$) are varied from 3 to 21 for $a_3 = 30$ (black line), 40 (magenta line), and 50 (cyan line) as shown in Fig. 6(a).
- **Main Pulse:** a_3 is varied from 10 to 90 for $a_1 = a_2 = 5$ (black line), 10 (magenta line), and 15 (cyan line) as shown in Fig. 6(b).

It is seen that proton acceleration strongly depends on a_1 and a_2. The peak energy reaches the maximum when a_1 and a_2 are smaller and gradually decreases with the increases in the values of a_1 and a_2 for all cases of a_3. Although, this decrements is rapid when $a_3 = 50$, however, the peak energy remains always higher. It can be explained by the fact that the target deforms rapidly due to the shock waves generated by the higher intensity oblique laser pulses, resulting in the higher transverse heating of electrons. The subsequent Rayleigh-Taylor instabilities then destroy the target. The main pulse then easily passes the target and no such merged proton layer

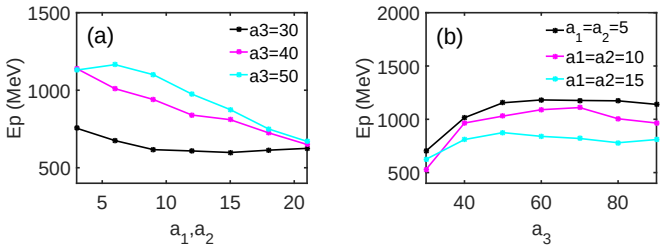

FIG. 7. Dependence of the proton peak energy: (a) on the oblique pulses ($a_1 = a_2$) for $a_3 = 30$ (black line), 40 (magenta line), and 50 (cyan line), and (b) on the main pulse (a_3) for $a_1 = a_2 = 5$ (black line), 10 (magenta line), and 15 (cyan line). The other parameters are the same as used in Fig. 1.

is found here. On the other hand, the peak energy increases with a_3 until 40 after that, it becomes almost constant. The reason is that for higher a_3 much of the laser pulse passes the target so that acceleration due to BOA is not possible.

VI. CONCLUSIONS AND DISCUSSIONS

In this paper, we have investigated the triple-laser pulses scheme to improve the proton beam quality with the help of particle-in-cell simulation. It has been shown that the proposed scheme not only enhance the proton beam energy but also decrease the beam energy spread and the beam divergence over that of the other schemes. The 2D PIC simulation results have shown that a high-quality proton beam of ∼1.2 GeV peak energy can be obtained using one order lower intense laser than that reported in table I. It has also been shown that the proton peak energy could be enhanced by about ∼ 250% and ∼ 150% while energy spread degraded by about ∼ 86% and ∼ 70% as compared with the SLP and DLP cases, respectively. It worth mention here that to generate a proton beam of GeV energy via SLP scheme we need a much higher intense laser pulse, i.e., $a \geq 100$, however, the obtained proton beam does not remain mono-energetic. The high energy proton beams with such reduced energy spread are desirable in practical applications such as laser-driven fast ignition and cancer treatment. The acceleration is driven due to the combination of several acceleration mechanisms. The main advantage of employing two oblique laser pulses is to form a microstructured target hence enhances the laser energy absorption. They also produce two separate hot electrons bunches that are merged into a small highly dense single bunch. The high intense self-focused main pulse then pushes the merged hot electrons bunch in the forward direction due to the enhanced radiation pressure. Therefore, this relativistic moving electron clouds drag the proton layer as a whole. As a result, the proton beam co-moves with the laser pulse henceforth can accelerate to very high energy due to the BOA. The influences of the individual laser

pulses on the proton acceleration have also been considered. It is found that the lower intense oblique pulses produce efficient proton acceleration while the acceleration is almost the same for $a_3 = 40 - 90$. We hope that the proposed scheme could be helpful to produce high-quality high-energetic proton beam using low-intensity laser pulses and might be an effective alternative for high-intensity laser pulses that are not currently attainable by the state-of-the-art laser technology.

ACKNOWLEDGMENTS

This work was supported by the National Natural Science Foundation of China (NNSFC) under Grant Nos. 11475147, 61627901, and 11875235 and the Fundamental Research Fund for Chinese Central Universities under Grant No. 2018FZA3004. The first author gratefully acknowledges the Chinese Scholarship Council for granting the CSC scholarship.

[1] S. V. Bulanov, T. Zh. Esirkepov, V. S. Khoroshkov, A. V. Kuznetsov, and F. Pegoraro, Phys. Lett. A **299**, 240 (2002).
[2] M. Roth, T. E. Cowan, M. H. Key, S. P. Hatchett, C. Brown, W. Fountain, J. Johnson, D. M. Pennington, R. A. Snavely, S. C. Wilks *et al.*, Phys. Rev. Lett. **86**, 436 (2001).
[3] K. W. D. Ledingham, J. Magill, P. McKenna, J. Yang, J. Galy, R. Schenkel, J. Rebizant, T. McCanny, S. Shimizu, L. Robson *et al.*, J. Phys. D: Appl. Phys. **36**, L79 (2003).
[4] M. Borghesi, J. Fuchs, S. V. Bulanov, A. J. Mackinnon, P. K. Patel, and M. Roth, Fusion Sci. Technol. **49**, 412 (2006).
[5] B. Dromey, M. Coughlan, L. Senje, M. Taylor, S. Kuschel, B. Villagomez-Bernabe, R. Stefanuik, G. Nersisyan, L. Stella, J. Kohanoff *et al.*, Nat. Commun. **7**, 10642 (2016).
[6] A. R. Smith, Med. Phys. **36**, 556 (2009); V. S. Khoroshkov and E. I. Minakova, Eur. J. Phys. **19**, 523, (1998).
[7] T. P. Yu, Y. Y. Ma, M. Chen, F. Q. Shao, M. Y. Yu, Y. Q. Gu, and Y. Yin, Phys. Plasmas **16**, 033112 (2009).
[8] H. Schwoerer, S. Pfotenhauer, O. Jäckel, K. -U. Amthor, B. Liesfeld, W. Ziegler, R. Sauerbrey, K. W. D. Ledingham, and T. Esirkepov, Nature **439**, 445 (2006).
[9] M. C. Levy, S. C. Wilks, M. Tabak, S. B. Libby, and M. G. Baring, Nat. Commun. **5**, 4149 (2014).
[10] D. B. Zou, H. B. Zhuo, T. P. Yu, H. C. Wu, X. H. Yang, F. Q. Shao, Y. Y. Ma, Y. Yin, and Z. Y. Ge, Phys. Plasmas **22**, 023109 (2015).
[11] Z. M. Zhang, X. T. He, Z. M. Sheng, and M. Y. Yu, Phys. Plasmas **17**, 043110 (2010).
[12] Z. M. Zhang, X. T. He, Z. M. Sheng, and M. Y. Yu, Phys. Plasmas **18**, 023110 (2011).
[13] L. Yin, J. Albright, B. M. Hegelich, and J. C. Fernández, Laser Part. Beams **24**, 291 (2006).
[14] L. Yin, B. J. Albright, B. M. Hegelich, K. J. Bowers, K. A. Flippo, T. J. T. Kwan, and J. C. Fernádez, Phys. Plasmas **14**, 056706 (2007).
[15] L. O. Silva, M. Marti, J. R. Davies, R. A. Fonseca, C. Ren, F. S. Tsung, and W. B. Mori, Phys. Rev. Lett. **92**, 015002 (2004); F. C. Wang, Chin. Phys. B **22**, 124102 (2013).
[16] C. -K. Huang, B. J. Albright, L. Yin, H. -C. Wu, K. J. Bowers, B. M. Hegelich, and J. C. Fernández, Phys. Plasmas **18**, 056707 (2011).
[17] X. Wang, W. Yu, E. Liang, and M. Y. Yu, Phys. Plasmas **19**, 053110 (2012).
[18] S. F. Tong, Z. M. Sheng, and M. Y. Yu, Phys. Plasmas **26**, 033103 (2019).
[19] O. Rahman, S. F. Tong, and Z. M. Sheng, Phys. Plasmas **27**, 033107 (2020).
[20] A. P. L. Robinson, D. Neely, P. McKenna, and R. G. Evans, Plasma Phys. Control. Fusion **49**, 373 (2007).
[21] K. Markey, P. McKenna, C. M. Brenner, D. C. Carroll, M. M. Günther, K. Harres, S. Kar, K. Lancaster, F. Nürnberg, M. N. Quinn *et al.*, Phys. Rev. Lett. **105**, 195008 (2010).
[22] G. G. Scott, J. S. Green, V. Bagnoud, C. Brabetz, C. M. Brenner, D. C. Carroll, D. A. MacLellan, A. P. L. Robinson, M. Roth, C. Spindloe *et al.*, App. Phys. Lett. **101**, 024101 (2012).
[23] C. M. Brenner, A. P. L. Robinson, K. Markey, R. H. H. Scott, R. J. Gray, M. Rosinski, O. Deppert, J. Badziak, D. Batani, J. R. Davies *et al.*, App. Phys. Lett. **104**, 081123 (2014).
[24] L. Yang, Z. G. Deng, M. Y. Yu, and X. G. Wang, Phys. Plasmas **23**, 083106 (2016).
[25] Y. J. Gu, Z. Zhu, Y. Y. Li, X. F. Li, C. Y. Chen, Q. Kong, and S. Kawata, EPL **95**, 35001 (2011).
[26] Y. J. Gu, Z. Zhu, X. F. Li, Q. Yu, S. Huang, F. Zhang, Q. Kong, and S. Kawata, Phys. Plasmas **21**, 063104 (2014).
[27] X. Zhang, B. Shen, X. Li, Z. Jin, F. Wang, and M. Wen, Phys. Plasmas **14**, 123108 (2007).
[28] W. Zhou, X. Hong, B. Xie, Y. Yang, L. Wang, J. Tian, R. Tang, and W. Duan, Phys. Rev. Accel. Beams. **21**, 021301 (2018).
[29] Y. Xu, J. Wang, X. Qi, M. Li, Y. Xing, L. Yang, and W. Zhu, Phys. Plasmas **24**, 033108 (2017).
[30] B. Qiao, M. Zepf, M. Borghesi, and M. Geissler, Phys. Rev. Lett. **102**, 145002 (2009).
[31] M. Chen, A. Pukhov, T. P. Yu, and Z. M. Sheng, Phys. Rev. Lett. **103**, 024801 (2009).
[32] J. Yu, W. Zhou, X. Jin, L. Cao, Z. Zhao, W. Hong, B. Li, and Y. Gu, Laser Part. Beams **30**, 307 (2012).
[33] J. Ferri, I. Thiele, E. Siminos, L. Gremillet, E. Smetanina, A. Dmitriev, G. Cantono, C. -G. Wahlström, and T. Fülöp, J. Plasma, Phys. **86**, 905860101 (2020).
[34] V. F. D'yachenko and V. S. Imshennik, Sov. J. Plasma Phys. **5**, 413 (1979); F. Brunel, Phys. Rev. Lett. **59**, 52, (1987).
[35] L. Cao, Y. Gu, Z. Zhao, L. Cao, W. Huang, W. Zhou, X. T. He, W. Yu, and M. Y. Yu, Phys. Plasmas **17**, 043103 (2010).